RSC Advances

ROYAL SOCIETY OF CHEMISTRY

www.rsc.org/advances

Cite this: DOI: 10.1039/c0xx00000x

www.rsc.org/xxxxxx

PAPER

Ag/Cu co-doped ZnS-In_2S_3 solid solutions: facile synthesis, theoretical calculations and enhanced photocatalytic activity

Jingxue Sun [a], Gang Chen*[a], Yujie Feng*[b] and Yu Wang [a]

Received (in XXX, XXX) Xth XXXXXXXXX 20XX, Accepted Xth XXXXXXXXX 20XX

DOI: 10.1039/b000000x

ZnS-In_2S_3 nano-spheres were prepared by a simple hydrothermal method without using any organic solvents or templates. In order to improve the photocatalytic performance, Ag and Cu were chosen as doping elements using for both single-doping and co-doping. The band structure, electronic structure and electron density were carefully investigated based on density functional theory (DFT). The roles of In and Ag/Cu in the solid solutions are found to be band adjusting, electron density control and electron mobility optimizing due to the d orbitals of Ag and Cu. Series of photocatalysts were further characterized by X-ray diffraction (XRD), scanning electron microscopy (SEM), UV-visible diffuse reflectance spectra (UV-vis) and Brunauer-Emmett-Teller (BET) surface area measurement. It is found that the formation of solid solution greatly broadened the light response range and made it possible for visible light responding. When the amount of Ag and Cu is 0.2 mL and 0.3 mL, the Ag/Cu co-doped ZnS-In_2S_3 solid solution showed the optimalizing value of 2.15 mmol·$h^{-1}g^{-1}$ under visible-light irradiation without using any noble metal as co-catalyst. After four cycles of photocatalytic tests, the activity showed barely decreasing.

Introduction

H_2 evolution *via* water splitting with renewable energy sources is a fascinating strategy from the view point of environmentally clean energy for the future. Among the H_2 evolution methods, photocatalytic water splitting using semiconductors as photocatalysts has caused wide attention since reported in 1972 and has been considered as one of the most growth potential ultimate solutions to energy and environmental issues[1-3]. Among the various kinds of photocatalyst oxide, especially TiO_2, is most widely studied because of its chemical stability, nontoxicity and high photocatalytic activity[4-6]. However, some shortcomings such as low solar efficiency hinder its extensive application. Therefore, one key route for H_2 evolution is water splitting using semiconductor photocatalysts under solar light. Among the metallic oxides, most of their valance bands consist of O 2p orbitals, which are relatively lower than the position of water oxidation. Compared to metallic oxide, sulfides, which have narrow band gaps (BGs) and valence bands at relatively negative potentials compared to oxides, can be used as good candidates for visible-light-driven photocatalysts due to the hybridization of O2p and S3p[7-12].

Till now, in order to adjust the bandgap of photocatalysts for the purpose of extending the absorption of light into the visible region, three main approaches have been widely used: (I) modification of the VB (valence band), (II) adjustment of the CB (conduction band), and (III) continuous modulation of the VB and/or CB [13, 14]. Cation doping and anion doping are the most widely used method for the VB and CB adjustment. In recent years, sulfide solid solutions have been extensively studied because of their continuous modulation of the VB and CB without introducing impurity levels and excellent performance for photocatalytic hydrogen production under visible light irradiation, such as ZnS-CdS [8, 11, 15-17], ZnS-$AgInS_2$ [18-20], ZnS-$CuInS_2$ [21, 22] and so on. Recently, we have reported that metal ions with d orbitals are beneficial to the narrowing of bandgap, such as Ag and Cu [23, 24]. Furthermore, to understand the structural and electronic properties of solid solutions, theoretical studies are desirable [25-27]. Few theoretical papers on solid solutions have appeared in the literature until recently.

In this work Ag and Cu are chose as co-doping element to adjust the bandgap of ZnS-In_2S_3 solid solution and standard density functional theory (DFT) calculations are also performed to study the influences of co-doping on band structures and electronic structures.

Experimental

Catalysts Preparation

In a typical process, $Zn(Ac)_2·2H_2O$ (0.6 mmol), $InCl_3·4H_2O$ (0.1 mmol), and thioacetamide (TAA) (2.4 mmol) were dissolved into 7.8 mL of pure water under magnetic stirring to form a clear solution (Solution A). $AgNO_3$ or $Cu(Ac)_2·2H_2O$ are chose as Ag or Cu source and are prepared to aqueous solution of 0.025 M (Solution B). Then Solution B was added dropwise into Solution A and then immediately transferred into an autoclave (Teflon cups with 15 mL inner volume). The autoclave was kept in the oven under 180 ℃ for 18 h and the cooled to room temperature. The product was collected by centrifugation, washed several times with absolute ethanol, and finally air dried.

Characterization

The structure of solid-solutions was analyzed by X-ray diffraction (XRD) on Rigaku D/max-2000 diffractometer (Cu Kα λ = 0.15406 nm). The morphology of the as-prepared samples was observed on FEI Quanta 200F field emission scanning electron microscope (FE-SEM). UV-Vis diffuse reflectance spectra were acquired by a spectrophotometer (TU-1900) and $BaSO_4$ was used as the reflectance standard.

The photocatalytic hydrogen generation test was performed in a gas-closed circulation system with a side quartz window. The as prepared powder was pre-dispersed by ultrasonication (100W) for 30 min in an aqueous solution (320 mL) containing Na_2SO_3 (1.2 $mol \cdot L^{-1}$) and Na_2S (0.1 $mol \cdot L^{-1}$) as electron donors. The reaction was carried out by irradiating the mixture with light from a Xe lamp (Trusttech PLS-SXE 300W, Beijing) which was equipped with an optical filter (λ>400 nm) to cut off the light in the ultraviolet region. The amount of produced H_2 was measured by gas chromatography (Agilent 6820) with a thermal conductivity detector (TCD) and Ar as the carrier gas.

Calculation method

The plane-wave pseudopotential method, based on density functional theory (DFT), was used to calculate the electronic structures for Ag/Cu co-doped solid solution by employing the CASTEP program[28], The generalized gradient approximation (GGA) in the scheme of Perdew–Burke–Ernzerhof (PBE) was used to describe the electronic exchange–correlation interactions[29] that is known to be an efficient and accurate scheme for solving the many-electron problem of a crystal[30]. The density of the Monkhorst-Pack *k*-point mesh are 6 × 6 × 6. The absorption curves can be obtained from the imaginary part of the dielectric constant from DFT calculation. The kinetic energy cut-off was set at 310 eV, and the geometric structures were first optimized by first-principle calculations. The Ag and Cu atom are substitute for zinc atoms in the crystal structure. The concentration of metal dopant was about 8%, comparable to the experimental value of 2%. During the structural optimizations, the cell shape and the positions of all atoms were allowed to be relaxed at an energy cutoff of 400 eV.

Results and discussion

Crystal Structure

Figure 1 shows the XRD patterns of ZnS-In_2S_3 solid solutions with different doping amount of Ag/Cu, which are denoted as Z-0, Z-0.1, Z-0.2, Z-0.3 and Z-0.5. As shown, the relatively broader peaks in pattern are attributed to the absence of long-range order in these samples and reflect the small particle size (ca. 20 nm from the Scherrer equation 1).

$$D = K\lambda/(B\cos\theta) \quad (1)$$

Where λ is the wavelength of X-ray radiation (0.154178 nm), K is the Scherrer's constant (K=0.9), θ is the diffraction angle and B is the full-width-at-half-maximum plane. The main diffraction peak positions of the obtained products can be easily indexed to ZnS, confirming the cubic zinc blende structure of the compounds. The main diffraction peaks matched with the cubic zinc blende structure. However, the hexagonal (wurtzite-type) structure was obtained with increasing of Cu/Ag value. The intensity of wurtzite reflection at 30.5 degree was found to increase with Cu/Ag content. No other impure peaks such as

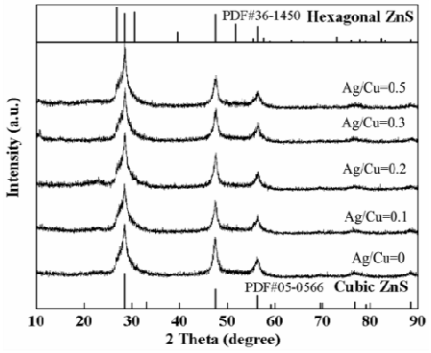

Figure 1 XRD patterns of samples with different amount of Ag/Cu

Ag_2S, CuS are observed, suggesting that Ag/Cu co-doping does not obviously change the crystalline structure of ZnS-In_2S_3 solid solution. This indicates that high purity products are synthesized. The molar ratio of metal ions in the samples confirmed by inductively coupled plasma (ICP) elemental analysis is shown in Table S1, indicating a high yield of the products.

Morphology

After hydrothermal treatment for 18 h under 180 ℃, the morphology of products are investigated by FE-SEM characterization, as shown in Figure 2. From the overall morphology of ZnS-In_2S_3 (Figure 2a), we can indicate that the sample is composed of numerous nearly-monodispersed spheres. The diameter of the spheres is around 200 nm (150-200 nm). Further observation (Figure 2b) shows that the sphere consists of numerous tiny particles with the size of tens of nanometers. The rough surface can provide more active sites which is benefit for the photocatalytic process. When Ag/Cu is doped into the ZnS-In_2S_3, the shape of the products remains to be spheres, while the size is obviously decreased. As shown in Figure 2c and 2d, the diameter of the sphere is 50-100 nm. As a result of the smaller size, the Brunauer-Emmett-Teller (BET) surface area is up to 76 m^2g^{-1}, which is much lager than pure ZnS (43 m^2g^{-1}) and ZnS-In_2S_3 (14 m^2g^{-1}). Meanwhile, the lager surface area means the more sufficient contact of the photocatalyst and the reaction agent.

UV-vis Diffuse Reflectance Spectra

Light absorbing properties are of importance for photocatalysts [24, 31] because the substitution of atoms into the lattice may result in noteworthy influence on the visible light responding. The UV-vis diffuse reflectance spectra of the samples with different amount of Ag/Cu co-doping are shown in Figure 3. The absorption edge of the ZnS-In_2S_3 is at 393 nm, corresponding to the bandgap of 3.15 eV, which is in UV light region. The steep edge also indicates that the absorption relevant to the bandgap is related to the intrinsic transition of the semiconductor and not to the transition from impurity levels[23, 32]. When Ag/Cu is doped into the lattice, the color of the product changes from white to light yellow, and the absorbance edge shows red-shift. Further increasing the doping amount, the absorption wavelength extended into the longer wavelength region, from 393 nm to 540 nm (Ag/Cu = 0.5 mL). According the formula (2), the bandgap energy of Z-0, Z-0.1, Z-0.2, Z-0.3 and

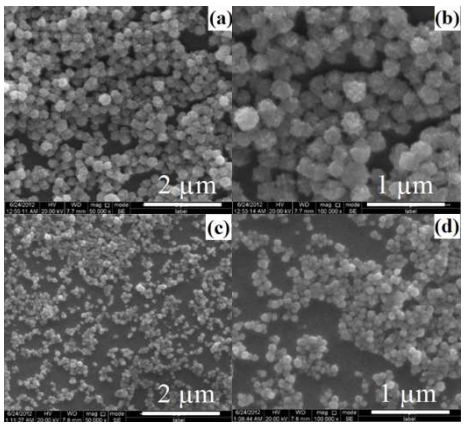

Figure 2 FE-SEM images of (a-b) ZnS-In_2S_3 solid solution and (c-d) Ag/Cu do-doped ZnS-In_2S_3 solid solution.

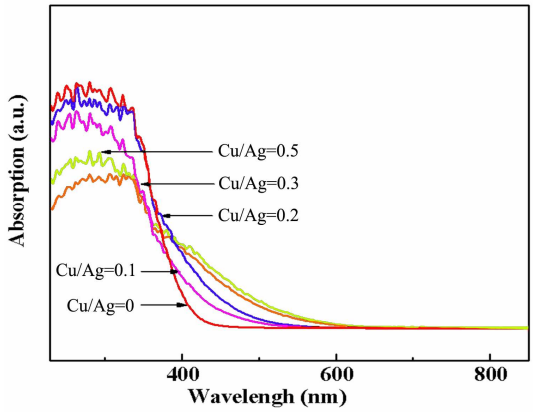

Figure 3 UV-Vis diffuse absorption spectra of the samples with different amount of Ag/Cu co-doping.

Z-0.5 are 3.15 eV, 2.98 eV, 2.71 eV, 2.53 eV and 2.30 eV, respectively.

$$E_g\,(\text{eV}) = 1240\,(\text{nm})/\lambda\,(\text{nm}) \quad (2)$$

E_g stands for the bandgap energy, λ stands for the light absorbance edge. The absorption shoulder of the diffuse reflectance spectra indicates that continuous levels are formed by the dopants in the forbidden band, which needs to be proved by theoretical calculations.

Photocatalytic Activities

The effect on the photocatalytic activity of Ag/Cu co-doping on ZnS-In_2S_3 solid solution samples prepared was systematically investigated. Figure 4 shows the dependence of photocatalytic activity on different amount of Ag/Cu. As shown, when no Ag or Cu is doped, the rate of hydrogen evolution is only 0.2 mmol·$h^{-1}g^{-1}$. When Ag is doped into the lattice, the rate shows obviously increasing (1.4 mmol·$h^{-1}g^{-1}$ for Ag = 0.1 mL and 1.65 mmol·$h^{-1}g^{-1}$ for Ag = 0.2 mL) under visible light irradiation (λ > 400 nm). It is also worth noting that when the amount of Ag further increases, the photocatalytic activity shows a trend of declining. The reason is suggested to be the recombined center induced by Ag. When Ag and Cu are co-doped into the lattice of the solid solution, the rate of photo-generated hydrogen is further improved compared with only Ag doping. As can be seen, when the amount of Ag and Cu is 0.2 mL and 0.3 mL, the maximum photocatalytic activity is achieved. The highest rate is calculated to be 2.15 mmol·$h^{-1}g^{-1}$,

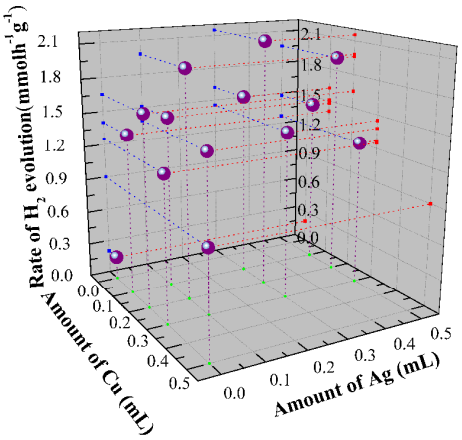

Figure 4 Rates of photocatalytic hydrogen evolution of the samples with different amount of Ag/Cu co-doping

which is more than ten times of ZnS-In_2S_3 solid solution. This means the synactic effects of Ag and Cu is benefit for the improving of photocatalysis.

In order to investigate the photo-stability of optimized photocatalyst Ag/Cu co-doped ZnS-In_2S_3 solid solution (Ag = 0.2 mL and Cu = 0.3 mL), a typical reaction time course for hydrogen evolution from an aqueous Na_2SO_3/Na_2S solution under visible light irradiation is carried out[33]. As shown in Figure S2, four runswere taken out and the reaction system was evacuated after each run. During the first run, the average hydrogen evolution rate can reach up to 2.05 mmol·$h^{-1}g^{-1}$. During the fourth run, the average rate is 1.85 mmol·$h^{-1}g^{-1}$, which means the photocatalyst shows good photo-stability under visible light irradiation. The decrease in the rate of hydrogen evolution might be related to the deactivation of the photocatalyst or attributed to the consumption of the sacrificial reagents in the solution.

Based on the previous report, the improved performances of photocatalysis may due to the following reasons: (1) Large surface area which leads to more sufficient contact and more active sites[34]; (2) Small particle size which leads to short migration time of photo-induced carriers[35]; (3) Appropriate band structure. Usually, large bandgap energy makes photocatalyst powerless in visible light responding and small bandgap energy can improve the ability of visible light responding. Meanwhile, too small band gap energy may cause the weak reducing ability of photo-generated electrons, which is adverse for the photocatalysis[36]; (4) Appropriate electron delocalization which means the favorable migration environment of photo-induced carriers[37]. Based on the above characterization and analysis, the obvious improvement of photocatalysis can attribute to reason (1) and (2). The effects of the latter two reasons are then further calculated by theoretical methods.

Band Structures and Electron Density

Band structures of ZnS and Ag/Cu co-doped ZnS-In_2S_3 were calculated based on density functional theory (DFT) in order to reveal the effects of In^{3+}, Cu^{2+} and Ag^{+} on the band structure of ZnS. Figure S1a and S1b (supplementary information) show the band structure of ZnS and Ag/Cu co-doped ZnS-In_2S_3, respectively. As can be seen, the top of the valance bands and the bottom of the conductive bands of both samples locate at G point, indicating that both compounds are direct band gap

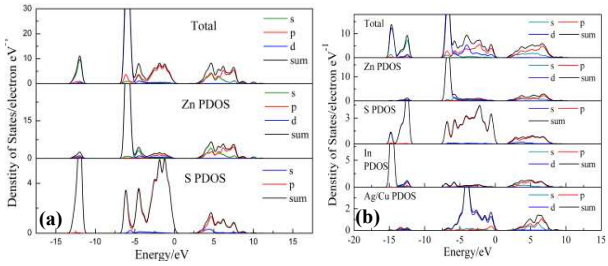

Figure 5 Density of states of (a) ZnS and (b) Ag/Cu do-doped ZnS-In_2S_3.

semiconductors, which is benefit for photocatalysts, also accordance with the UV-vis analysis. Figure 5 shows the density of states (DOS) and partial density of states (PDOS). As shown in Figure 5a, both of the conduction and valence bands of ZnS consisted of the hybrid orbitals of Zn and S due to the covalency. The conduction band of ZnS consists of Zn 4s4p orbitals and S 3p orbital contributes to the vanlace band of ZnS, similar as the results reported[12, 38, 39]. The bandgap energy calculated from theband structure and DOS is 2.4eV, which is smaller that the bandgap energy obtained from the UV-vis analysis. This is a common feature of DFT calculations [40], also an artifact of the GGA method used for this calculation [33, 41]. For Ag/Cu co-doped ZnS-In_2S_3, as shown in Figure 5b, the bandgap energy is reduced to 1.25 eV. The narrower bandgap is due the hybridized orbital induced by In, Ag and Cu. As shown in Figure 5b, the bottom of CB moves to low energy level due to the hybridization of Zn d orbital and In d orbital, while the In d orbital barely contribute to the top of VB. The top of valance band moves to high energy which because the introducing of d orbitals of Ag and Cu. Therefore, the band gap is narrowed due to the formation of hybridized orbitals, as described in Figure 6.

Furthermore, the conduction band is broadened after the introducing of In, Ag and Cu, meaning that the delocalization of electron is improved. The broadened conduction band is consist of In 5s5p and Zn 4s4p, indicating that the broadened phenomenon is mainly due to the effect of In, while the d orbitals of Ag and Cu attribute to the shift of the valance band. Meanwhile, the stepwised red-shifting of the absorbance edge and continuous CB bottom and VB top further confirmed the formation of solid solution. Thus can be seen, the changing of H_2 production rate on the Ag/Cu could be due to the tailoring of band structure and light absorbance. When Ag/Cu was induced into the lattice, the band gap is reduced due to the continuous expanding of VB, which is accordance with the UV-vis spectra analysis in Figure 3.

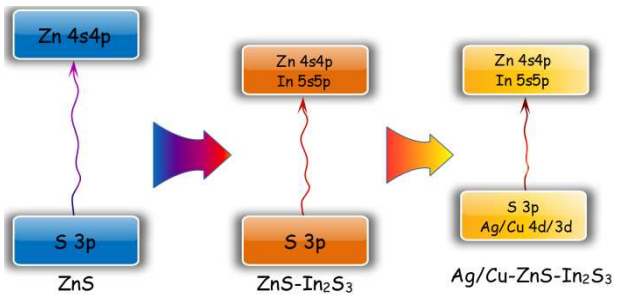

Figure 6 The evolution of band gap corresponding to the introducing of In and Ag/Cu.

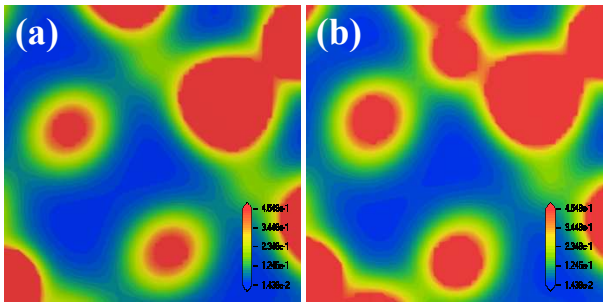

Figure 7 Electron densities of (a) ZnS and (b) Ag/Cu do-doped ZnS-In_2S_3.

The band gap energy mainly contributes to the light absorbance of the photocatalysts, while the electron density also has an effect on the activity of photocatalyst and is useful to discuss the origin of the narrow band gap of visible-light responsive photocatalysts. Plotted electron densities around cation atoms are shown in Figure 7. As shown, when In and Ag/Cu was present in the crystal lattice of ZnS, this type of impurity plays the role of donor energy level. The co-doped solid solution has more electron-carriers compared with pure ZnS. Also, the CB width is obviously broadened. Furthermore, except for carriers, the electron delocalization is proved, which is also favorable for the photo-induced electron transportation. Therefore, this type of doping could obviously enhance the photocatalytic performance of under visible-light irradiation.

Conclusions

In summary, ZnS-In_2S_3 solid solution was synthesized by a simple hydrothermal method without using any organic templates or solvents. The formation of solid solution greatly broadened the light response range and made it possible for visible light responding. The method of Ag/Cu co-doping into the solid solution further improved the photocatalytic performances for hydrogen evolution. Theoretical calculation indicated that the incorporation of Ag/Cu expanded the VB and adjusted the electron density. The enhance activity is supposed to be due to the large surface area, small particle size and appropriate band structure and electron density. When the amount of Ag and Cu is 0.2 mL and 0.3 mL, the maximum photocatalytic activity is achieved (2.15 $mmol \cdot h^{-1}g^{-1}$), which was more than ten times of ZnS-In_2S_3 solid solution. After four cycles of photocatalytic tests, the activity showed barely decreasing.

Acknowledgement

This work was financially supported by the National Nature Science Foundation of China (21271055). We acknowledge for the support by Fundamental Research Funds for the Central Universities (HIT. IBRSEM. A.201410), Open Project of State Key Laboratory of Urban Water Resource and Environment，Harbin Institute of Technology (No. QAK201304) and Program for Innovation Research of Science in Harbin Institute of Technology (B201412).

Notes and references

[a] *Department of Chemistry, Harbin Institute of Technology, Harbin 150001, P. R. China; E-mail:gchen@hit.edu.cn*

[b] State Key Laboratory of Urban Water Resource and Environment, Harbin Institute of Technology, Harbin 150001, P. R. China; E-mail: yujief@hit.edu.cn

† Electronic Supplementary Information (ESI) available: See DOI: 10.1039/b000000x/

1. A. Fujishima and K. Honda, Nature, 1972, 238, 37-38.
2. Y. P. Li, J. Zhan, L. Y. Huang, H. Xu, H. M. Li, R. X. Zhang and S. L. Wu, Rsc Advances, 2014, 4, 11831-11839.
3. T. N. He, X. L. Guo, K. Zhang, Y. M. Feng and X. D. Wang, Rsc Advances, 2014, 4, 5880-5886.
4. S. Sakulkhaemaruethai and T. Sreethawong, Int. J. Hydrogen Energy, 2011, 36, 6553-6559.
5. R. Zhao, R. F. Ding, S. J. Yuan, W. Jiang and B. Liang, Int. J. Hydrogen Energy, 2011, 36, 1066-1073.
6. J. X. Sun, G. Chen, Y. X. Li, R. C. Jin and Q. Wang, Energy Environ. Sci., 2011, 4, 4052-4060.
7. X. W. Wang, G. Liu, L. Z. Wang, Z. G. Chen, G. Q. Lu and H. M. Cheng, Advanced Energy Materials, 2012, 2, 42-46.
8. S. A. Macias-Sanchez, R. Nava, V. Hernandez-Morales, Y. J. Acosta-Silva, L. Gomez-Herrera, B. Pawelec, S. M. Al-Zahrani, R. M. Navarro and J. L. G. Fierro, Int. J. Hydrogen Energy, 2012, 37, 9948-9958.
9. F. Z. Jia, Z. P. Yao and Z. H. Jiang, Int. J. Hydrogen Energy, 2012, 37, 3048-3055.
10. D. Barpuzary, Z. Khan, N. Vinothkumar, M. De and M. Qureshi, J. Phys. Chem. C, 2012, 116, 150-156.
11. X. Xu, R. J. Lu, X. F. Zhao, S. L. Xu, X. D. Lei, F. Z. Zhang and D. G. Evans, Appl. Catal. B-Environ., 2011, 102, 147-156.
12. N. S. Chaudhari, S. S. Warule and B. B. Kale, Rsc Advances, 2014, 4, 12182-12187.
13. H. Tong, S. X. Ouyang, Y. P. Bi, N. Umezawa, M. Oshikiri and J. H. Ye, Adv. Mater., 2012, 24, 229-251.
14. M. Pal, S. Bera, S. Sarkar and S. Jana, Rsc Advances, 2014, 4, 11552-11563.
15. K. Ikeue, S. Shiiba and M. Machida, ChemSusChem, 2011, 4, 269-273.
16. M. C. Liu, L. Z. Wang, G. Q. Lu, X. D. Yao and L. J. Guo, Energy Environ. Sci., 2011, 4, 1372-1378.
17. K. Zhang, D. W. Jing, Q. Y. Chen and L. J. Guo, Int. J. Hydrogen Energy, 2010, 35, 2048-2057.
18. S. J. Zhang, Rsc Advances, 2014, 4, 15835-15840.
19. H. Xu, J. X. Zhu, Y. X. Song, W. K. Zhao, Y. G. Xu, Y. H. Song, H. Y. Ji and H. M. Li, Rsc Advances, 2014, 4, 9139-9147.
20. T. A. Arun, D. K. Chacko, A. A. Madhavan, T. G. Deepak, G. S. Anjusree, T. Sara, S. Ramakrishna, S. V. Nair and A. S. Nair, Rsc Advances, 2014, 4, 1421-1424.
21. W. J. Zhang and X. H. Zhong, Inorg. Chem., 2011, 50, 4065-4072.
22. H. W. Huang, S. B. Wang, N. Tian and Y. H. Zhang, Rsc Advances, 2014, 4, 5561-5567.
23. Y. X. Li, G. Chen, Q. Wang, X. Wang, A. K. Zhou and Z. Y. Shen, Adv. Funct. Mater., 2010, 20, 3390-3398.
24. Y. X. Li, G. Chen, C. Zhou and J. X. Sun, Chem. Commun., 2009, 2020-2022.
25. H. S. Park, K. E. Kweon, H. Ye, E. Paek, G. S. Hwang and A. J. Bard, J. Phys. Chem. C, 2011, 115, 17870-17879.
26. S. Kawasaki, K. Akagi, K. Nakatsuji, S. Yamamoto, I. Matsuda, Y. Harada, J. Yoshinobu, F. Komori, R. Takahashi, M. Lippmaa, C. Sakai, H. Niwa, M. Oshima, K. Iwashina and A. Kudo, J. Phys. Chem. C, 2012, 116, 24445-24448.
27. J. Nisar, B. C. Wang, C. M. Araujo, A. F. da Silva, T. W. Kang and R. Ahuja, Int. J. Hydrogen Energy, 2012, 37, 3014-3018.
28. O. Jepsen, O. K. Andersen and A. R. Mackintosh, Phys. Rev. B, 1975, 13, 3060-3083.
29. J. P. Perdew, K. Burke and M. Ernzerhof, Phys. Rev. Lett., 1996, 77, 3865-3868.
30. P. Hohenberg and W. Kohn, Phys. Rev., 1964, 136, 864-871.
31. Y. X. Li, G. Chen, H. J. Zhang, Z. H. Li and J. X. Sun, J. Solid State Chem., 2008, 181, 2653-2659.
32. H. X. Zhao, H. T. Yu, X. Quan, S. Chen, H. M. Zhao and H. Wang, Rsc Advances, 2014, 4, 624-628.
33. H. L. Hou, L. Wang, F. M. Gao, G. D. Wei, J. J. Zheng, B. Tang and W. Y. Yang, Rsc Advances, 2014, 4, 19939-19944.
34. Z. W. Luo, H. Jiang, D. Li, L. Z. Hu, W. H. Geng, P. Wei and P. K. Ouyang, Rsc Advances, 2014, 4, 17797-17804.
35. H. Kato, K. Asakura and A. Kudo, J. Am. Chem. Soc., 2003, 125, 3082-3089.
36. M. Xu, J. T. Zai, Y. P. Yuan and X. F. Qian, J. Mater. Chem., 2012, 22, 23929-23934.
37. B. Kumar, S. Saha, A. Ganguly and A. K. Ganguli, Rsc Advances, 2014, 4, 12043-12049.
38. Y. D. Liu, L. Ren, X. Qi, Y. Wang, X. J. Liu and J. X. Zhong, Rsc Advances, 2014, 4, 8772-8778.
39. B. Weng, S. Q. Liu, Z. R. Tang and Y. J. Xu, Rsc Advances, 2014, 4, 12685-12700.
40. Y. X. Li, G. Chen, H. J. Zhang and Z. H. Li, Mater. Res. Bull., 2009, 44, 741-746.
41. J. W. Liu, G. Chen, Z. H. Li and Z. G. Zhang, J. Solid State Chem., 2006, 179, 3704-3708.